WILEY

Research Article

Ductile Failure Modes of Double Shear Steel-to-Wood Dowel Type Connections

Emanuele Maiorana [iD],[1] Guillaume Hervé Poh'sié [iD],[2,3] and Tegha Maxima Enah [iD][4]

[1]Department of Economics, Science, Engineering and Design, University of the Republic of San Marino, Via Consiglio dei Sessanta 99, Dogana 47891, San Marino
[2]College of Technology, University of Buea, Buea, Cameroon
[3]Institut Supérieur des Technologies Avancées (ISTA-IUG), Ndokotti, Douala, Cameroon
[4]Department of Civil Engineering, National Advanced School of Public Works, Yaoundé, Cameroon

Correspondence should be addressed to Tegha Maxima Enah; teghamaximaenah@gmail.com

To analyze the behavior of typical hybrid steel–wood connections in wooden buildings, 3D continuum-based finite element analysis (FEA) models of the most critical connections were developed using the Abaqus/CAE program. Accurate modeling requires appropriate element and material formulations, as well as proper contact definitions between connection components. To address the asymmetric behavior of bilinga wood, the Hill criterion, coupled with a pressure overclosure relationship, was employed to control ductile yielding and brittle fracture near bolt holes. Yielding of the steel components, such as bolts and slotted in plates, was captured using the Von Mises criterion. Model validation was performed indirectly by comparing the numerical results with experimental tests conducted on wood and through theoretical comparisons of bolt failure modes according to Eurocode 5. The developed models satisfactorily replicated bolt failure, including yielding in both steel and wood members. Parametric studies revealed that staggered bolt configurations have enhanced ductility and moment-resisting capacity than single-row bolt arrangements. Additionally, a solution involving a gap of 10 mm between slotted in base plates and timber columns was introduced to evaluate the performance and ultimate load capacity of these connections.

Keywords: Bilinga wood; dowel-type connection; experimental results; finite element analysis; numerical simulations; steel-to-wood

1. Introduction

Growing calls from the United Nations to decarbonize the building sector, in an effort to combat climate change and build more sustainable cities, have led to a significant increase in the construction of wooden buildings over the past decade. As wooden buildings gain popularity due to their positive environmental impact and contribution to a sustainable future [1], understanding the behavior of connections between structural members in these structures becomes critical in ensuring their safety and performance. Connections are the weakest points in wooden buildings, governing their load-carrying capacity, stiffness, and stability [2–4]. They are critical components in

wooden structures and are responsible for over 25% of collapses worldwide [5, 6]. The traditional approach of studying the behavior of these connections through experimental testing is limited by cost, time, expertise, and the number and types of configurations that can be tested. This presents a significant challenge, particularly in developing countries where resources for full-scale experiments are often scarce. Given these limitations, there is a need for complementary and efficient methods to study the behavior of timber connections to keep pace with the increasing demand for timber construction.

To analyze the behavior of connections in wooden buildings, three specific objectives will be pursued. These objectives include (1) the development of accurate finite element models

capable of reliably simulating the behavior of wooden connections, (2) the investigation of the load-bearing capacity, stress distributions, and failure modes of selected wood connections, and (3) the evaluation of the influence of connection geometry and bolt arrangement on the global behavior of wood connections.

Three main types of connections used in wooden buildings are as follows: carpentry, glued, and mechanical. The latter, which is the focus of this study, transmits forces through the juxtaposition of the connected members. Mechanical connections typically contain fasteners made of steel or other materials and are the most common and widely used type of wood connections in construction. Furthermore, mechanical connections can be categorized into two main types: dowel-type and bearing-type connections [7, 8]. Additionally, there are hanger-type connections that transmit loads through the combination of bearing and dowel-type fasteners [7].

A dowel is a generic term used for a fastener that transfers load between connected members through a combination of bending, shear in the dowel, and bearing in the wood [8]. These connections transmit both lateral loads and withdrawal loads. Lateral loads are transmitted by bearing stresses developed between the fastener and the members of the connection, while withdrawal loads parallel to the fastener axis are transmitted through friction or bearing to the connected members [7]. Metal plate connections also fall into the category of dowel-type connections.

The overall behavior of dowel-type connections is influenced by several factors, including the anchoring properties of the wood, the nature and type of fastener, and the geometry and type of load applied on the connection [9]. Based on the load-slip curves by Racher et al. [10], the global behavior of wooden connections loaded in tension varies from brittle in glued connections to perfectly elastoplastic in nailed connections loaded in tension parallel to the grain.

Most building standards, including Eurocode 5, National Design Specification (NDS) [11], and the Canadian Wood Council (CWC), assume ductile failure of wood connections in their design rules. These rules are based on the work done by Johansen [12] in his theoretical model. Johansen [12] assumed that the bending or yielding failure of the fastener through the formation of one or more plastic hinges and the embedment failure of the wood beneath the fasteners is ductile. Figure 10.1 of [13] illustrates the ductile failure modes of a single and double shear wood-to-wood connection.

Brittle failure modes can still occur in wood even when detailing rules are followed during the design. Wood connections can fail prematurely before achieving their ductile capacity. This implies that brittle failures can arise due to wood failure before the fasteners enter the plastic range, resulting in a sudden collapse of the connection. These brittle failure modes are typically caused by a combination of shear parallel to the grain and tension perpendicular to the grain in wood. Figure 4.26 of [14] illustrates the brittle failure modes of wood connections.

The possible failure modes of bolted steel-to-wood connections in double shear, such as those between a timber column and a concrete column are (f)(h) in Figure 10.2 of [13].

2. Numerical Analysis

The Abaqus software package, ver. 2020, is used for numerical modeling and two geometrical approximations are applied to the connections:

1. Typically, bolted wooden connections are made with a 1 mm clearance in the holes to overcome challenges posed by slim margins in aligning holes and fitting bolts. However, since contact interactions in Abaqus are defined between elements that touch, defining interactions between the bolts and interior walls of the holes can lead to convergence problems or numerical singularity issues. To avoid this, the dimensions of the holes are set equal to those of the bolts.

2. An additional simplification is applied to the bolts and their components. In physical models, bolts are threaded across the entire length of the shank. While modeling threads is possible, creating this geometry for both and holes is time-consuming and results in extra nodes, complicating analysis. To simplify the analysis, the bolt shanks are modeled as solid cylinders, and frictional contact is established between the bolts and holes. Furthermore, the nuts, shanks, and washers are combined into a single solid element, as the physical models show no evidence of the nuts being torn off. This eliminates the need to define contacts between the nuts, heads, and bolt shanks.

Figure 8 of [15] illustrates the Lamé function, which accounts for the contact pressure–deformation relationship. The nonlinear relationship between the normal pressure and the deformation (overclosure) is given by Equation (1), and a similar relationship is employed by Hassanieh et al. [15].

$$\left(\frac{u_{\text{inter}}}{u_0}\right)^{n_0} + \left(\frac{\sigma_0 - \sigma_{\text{L}}}{\sigma_0}\right)^{n_\sigma} = 1, \tag{1}$$

where n_0, n_σ are the positive numbers that control the function curvature, $n_0 = 3.9$ and $n_\sigma = 1.1$; u_{inter} is the deformation or overclosure; u_0 is the contact deformation, $u_0 = 0.45$ mm for bolted connections; σ_0 is the maximum compressive strength of the timber; and σ_{L} is the normal pressure at the surface.

Abaqus employs a pure master–slave contact algorithm to simulate the behavior at the contact surfaces. Eight-node (hexahedral) brick elements with reduced integration formulation are used for the timber members, while C3D6 are used for the bolts in the model. These elements contain more nodes than individual tetrahedrons, but provide a coarser mesh discretization, reducing the computational time without sacrificing accuracy [16].

Additionally, a very fine mesh is applied near the holes in the wood members, while a slightly coarser mesh is used in parts of the member far away from the hole. Fixed external support conditions are applied at the column bases to prevent any displacement or rotation. The load is introduced numerically by applying a maximum displacement of 50 mm

monotonically, at the end beams or top of the column in the vertical direction of the coordinate system.

The steel material is modeled as a nonlinear isotropic, with Young's modulus and Poisson's ratio obtained from literature. The Von Mises yield criterion is used to model the evolution of plasticity in the bolts and steel plates until the formation of plastic hinges. The hardening of the steel fasteners does not influence the behavior of the connection [17].

Wood is modeled as an orthotropic material by defining engineering constants in the property module of Abaqus. An elastic-perfectly plastic material model with strain hardening is used for wood in compression perpendicular and parallel to the grain. The evolution of plastic deformations of wood beneath the fasteners and the entire material is taken into account using the Hill 3D yield criterion. The Hill criterion describes anisotropic yielding [18], and is a generalized form of the Von Mises criterion extended to anisotropic materials (Equation (2)).

$$f(\sigma) = F(\sigma_{22} - \sigma_{33})^2 + G(\sigma_{33} - \sigma_{11})^2 + H(\sigma_{11} - \sigma_{22})^2 \\ + 2L\sigma_{23}^2 + 2M\sigma_{31}^2 + 2N\sigma_{12}^2,$$

(2)

with:

$$F = \frac{1}{2}\left(\frac{1}{R_{22}^2} + \frac{1}{R_{33}^2} - \frac{1}{R_{11}^2}\right),$$

$$G = \frac{1}{2}\left(\frac{1}{R_{33}^2} + \frac{1}{R_{11}^2} - \frac{1}{R_{22}^2}\right),$$

$$H = \frac{1}{2}\left(\frac{1}{R_{11}^2} + \frac{1}{R_{22}^2} - \frac{1}{R_{33}^2}\right),$$

$$L = \left(\frac{3}{2R_{23}^2}\right), M = \left(\frac{3}{2R_{13}^2}\right), N = \left(\frac{3}{2R_{12}^2}\right),$$

$$R_{11}^2 = \left(\frac{f_{c11}}{f^0}\right), \ R_{22}^2 = \left(\frac{f_{c22}}{f^0}\right), \ R_{33}^2 = \left(\frac{f_{c33}}{f^0}\right),$$

$$R_{12}^2 = \left(\frac{f_{v12}}{\tau^0}\right), R_{13}^2 = \left(\frac{f_{v13}}{\tau^0}\right), R_{23}^2 = \left(\frac{f_{v23}}{\tau^0}\right),$$

and

$$\tau = \frac{f^0}{\sqrt{3}},$$

where F, G, H, and L are combination constants of yield stress ratios; R_{ij} are the yield ratios for normal or shear stress component to the reference yield stress; f_{c11} is the compressive strength parallel to the grain; f_{c22} and f_{c33} are the compressive strength perpendicular to the grain; f^0 is the reference yield stress.

Numerical parametric studies will be conducted to evaluate the influence of some geometric parameters on the global
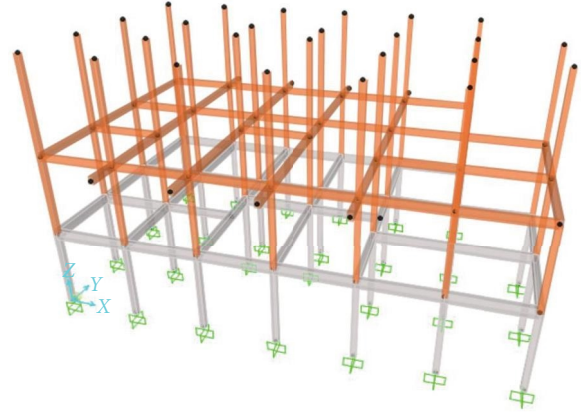

FIGURE 1: Structural model of the building.

behavior of wood connections. These studies will include investigations into the bolt arrangements and the influence of gaps between the components of the wood connections.

3. Cases Study

3.1. Geometry. Post-and-beam buildings utilize large sawn lumber, glulam, or structural composite lumber (SCL) to transmit loads from one storey to another. Due to the size of the structural frame elements, the building used as a case study qualifies as a post-and-beam structure. The example building is a modern residential home consisting of a reinforced concrete (RC) basement topped with an RC slab. Above the basement, a wood-framed floor supports a livable attic roof that contains the building's main private living areas. Additionally, the basement walls are constructed with hollow concrete blocks, while the wooden floor walls are made of SCL panels and tempered glass.

Figure 1 illustrates a simplified structural model of the building. Although, the structural elements of the roof are not explicitly modeled, the actions of these elements are accounted for as point loads on the columns of the livable attic.

3.2. Connections in the Building. The main connections influencing the global stability of the structure include the following: the timber roof beams to wooden columns, the double timber beams to columns, and the timber bases to concrete columns. The connections between RC columns and beams, as well as between RC columns and footings are not considered in this study, as they are subject of a separate numerical investigation. Figure 2 illustrates the geometry of the connection between the wooden roof beam and the column. Figure 3 depicts the geometry of the wooden double beam-to-column connection. Figure 4 presents the geometry of the wooden column base.

The geometric characteristics of the most stressed wooden beam are presented in Table 1.

3.3. Material Characteristics. The material characteristics include the properties of wood, concrete, reinforcing steel, steel plates, bolts, and anchor studs used in the building. The wood characteristics encompass the strength and elastic properties of *Nauclea diderrichii* (commonly known as bilinga wood), which is used as a building material. The strength properties of the
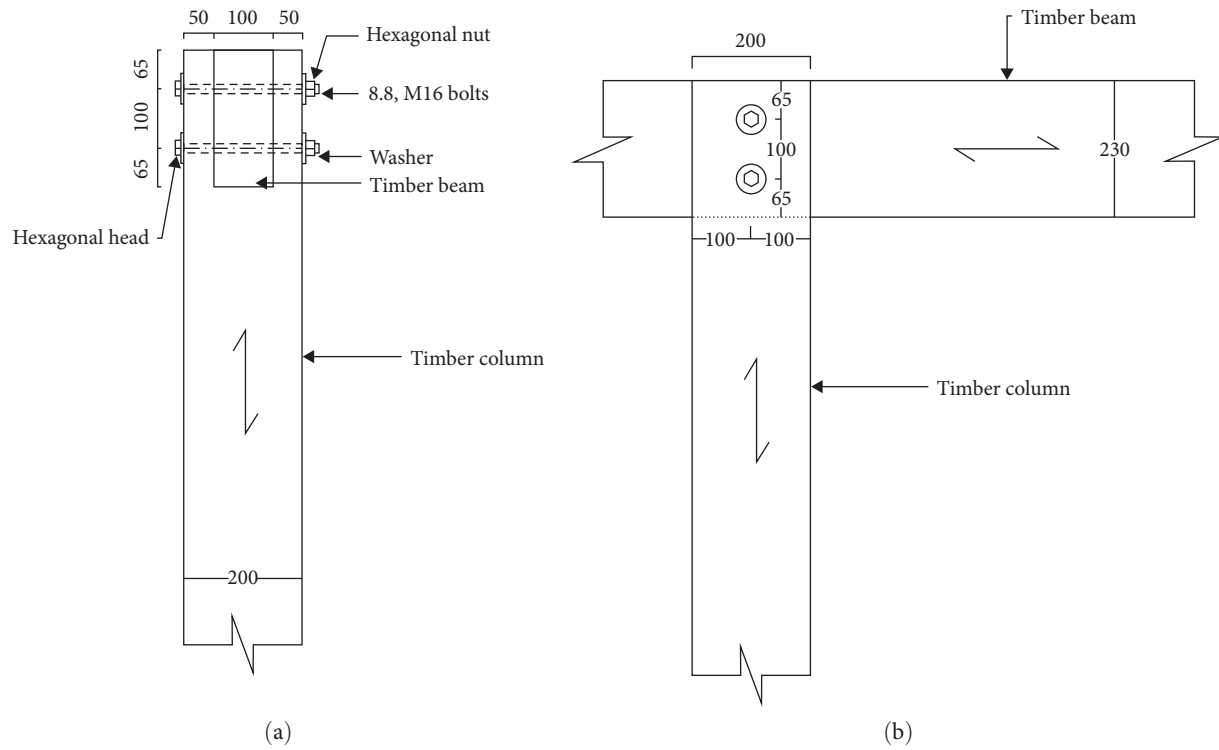
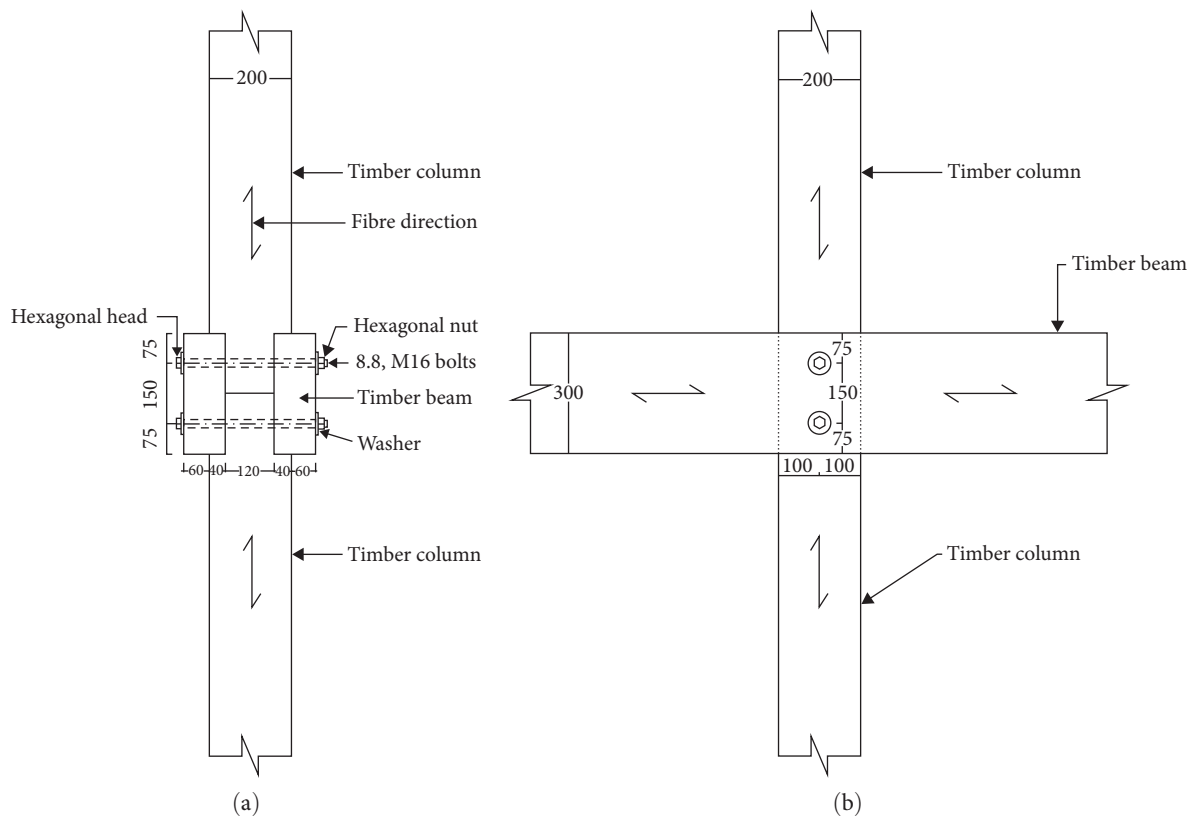FIGURE 2: Timber roof beam-to-column connection (mm). (a) Front view and (b) side view.

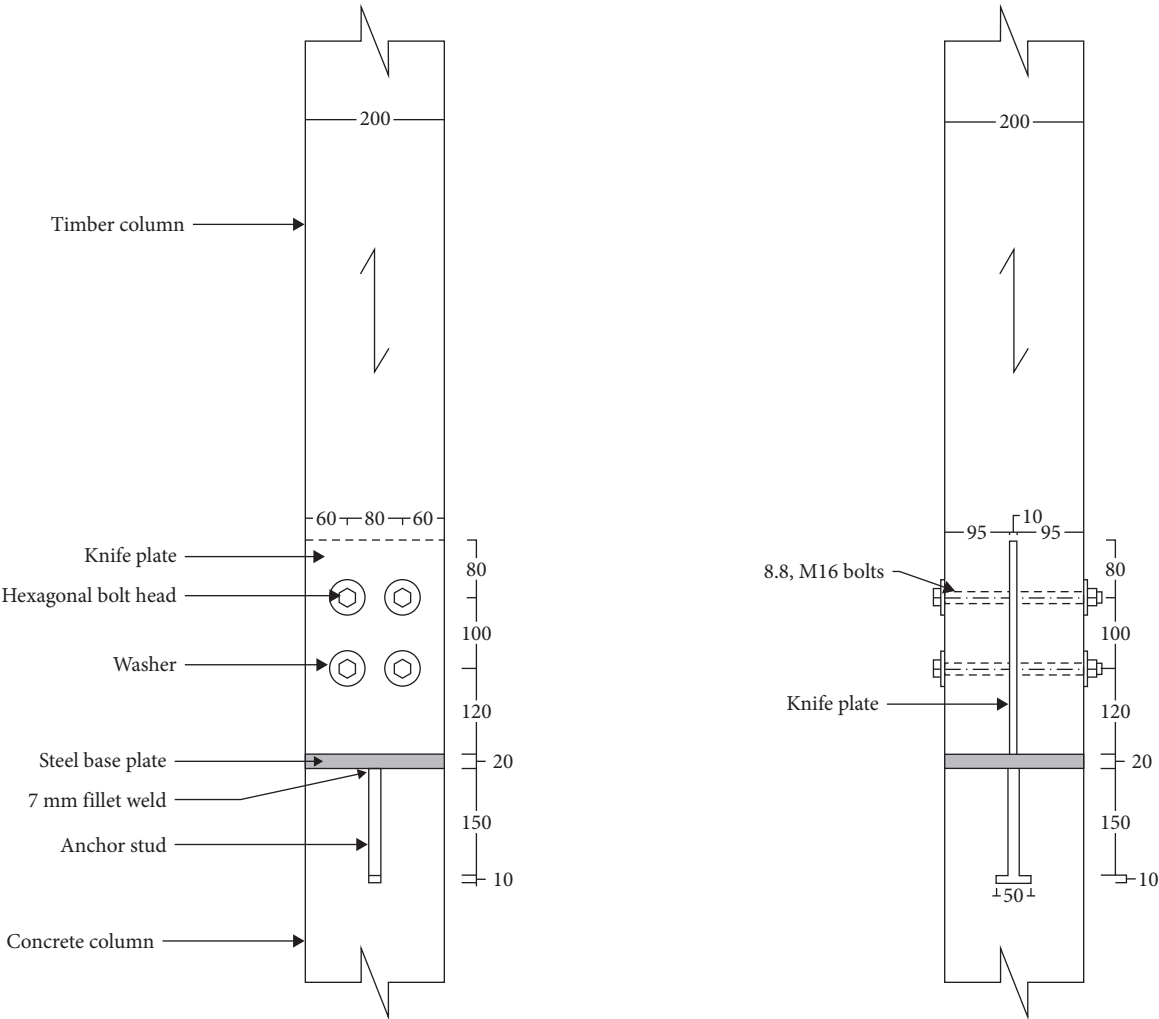FIGURE 3: Timber double beam-to-column connection (mm). (a) Front view and (b) side view.

FIGURE 4: Timber column base connection (mm).

TABLE 1: Geometric characteristics of wooden beam.

Designation	Expression	Value	Unit
Base	b	200	mm
Height	h	300	mm
Maximum simply supported span	l	4.65	m
Moment of inertia	$I_{g,y}$	450,000,000.00	mm^4
Section modulus	W	3,000,000.00	mm^3
Influence area	l_{beam}	2.95	m

wood are presented in Table 2, while the elastic properties at 12% humidity are provided in Table 3.

The steel characteristics used for the knife and base plate are provided in Table 4. The mechanical properties of steel bolts used in the connections are detailed in Table 5.

The load combinations considered for the wooden main beam generated solicitations such as bending moment, shear, and axial force. A maximum bending moment of 6.72 kN was obtained from load combination 3. Additionally, a maximum shear force of 2.90 kN was also achieved from this combination.

The largest axial force of 104.47 kN was obtained from load arrangement 4.

4. Numerical Models

Numerical investigations have been conducted on three main connections present in the case study building, including some parametric studies on these connections that are commonly used and are found in many buildings. The parametric studies allowed to explore potential improvements to these existing connections, identify novel situations, and significantly enhance the performance of these widely used connections.

4.1. Beam-to-Column Connection. Two numerical models, namely connection A and connection B, were created for the roof beam-column connection by varying the geometrical arrangements of bolts. The components in these models were meshed with 3D finite elements that support geometry and material nonlinearity. The wooden elements were meshed with C3D8R hexahedron elements, while C3D6 wedge elements (6-node linear triangular prism elements) were used to mesh the bolt. These elements were chosen because they strike a balance between computational efficiency and accuracy,

TABLE 2: Strength properties of the wood [19].

Properties	Strength class Expression	D50 Value
Strength properties (N/mm^2)		
Bending	$f_{m,k}$	50
Tension parallel to the grain	$f_{t,0,k}$	30
Tension perpendicular to the grain	$f_{t,90,k}$	0.6
Compression parallel to the grain	$f_{c,0,k}$	29
Compression perpendicular to the grain	$f_{c,90,k}$	9.3
Shear parallel to the grain	$f_{v,k}$	4
Rolling shear	$f_{v,k,r}$	0.92
Stiffness properties (kN/mm^2)		
Mean modulus of elasticity parallel to bending	$E_{0,mean}$	14
5 percentile modulus of elasticity parallel to bending	$E_{0.05}$	11.8
Mean modulus of elasticity perpendicular	$E_{90,mean}$	0.93
Mean shear modulus	G_{mean}	0.88
Density (kg/m^3)		
5 percentile density	ρ_k	620
Mean density	ρ_{mean}	750

TABLE 3: Elastic properties of wood at 12% humidity.

Property	Expression	Value	Unit
MOE along the longitudinal direction	E_{11}	14,660	N/mm^2
MOE along the radial direction	E_{22}	2536.18	N/mm^2
MOE along the tangential direction	E_{33}	1876.48	N/mm^2
	ν_{12}	0.15	—
Poisson ratios	ν_{13}	0.2	—
	ν_{23}	0.25	—
	G_{12}	1495.32	N/mm^2
Shear modulus	G_{13}	1260.76	N/mm^2
	G_{23}	498.4	N/mm^2

TABLE 4: Mechanical properties of the knife and base plate of the connection to the base of the column.

Property	Expression	Value	Unit
Steel class	—	S275JR	—
Yield strength	γ_s	275	N/mm^2
Ultimate strength	γ_u	430	N/mm^2
Modulus of elasticity	E	210,000	N/mm^2
Poisson ratio	ν	0.3	—

allowing for a finer mesh size across the timber members without excessive computational cost. This approach ensured that the timber members were adequately resolved, particularly in regions of interest, such as the bolt-hole areas. To address potential compatibility issues between the C3D8R and C3D6 elements, careful attention was paid to mesh sizing and node alignment. The mesh size for the C3D8R elements was designed to closely match that of the C3D6 elements near the bolts ensuring a smooth transition between the two regions.

The finite element mesh for both connections was divided into several subregions with varying finite element sizes to account for estimated areas of higher local stress concentration. These resulted in 102,625 and 99,422 finite elements for connection A and connection B. Additionally, a maximum mesh size of 9.5 mm was used in both models. The numerical models of connections A and B are illustrated in Figures 5 and 6, respectively.

Moment-rotation curves for connections A and B were plotted to evaluate their load-bearing capacities and overall behavior. As shown in Figure 7, these curves were obtained by applying a monotonic increasing displacement of 50 mm at the end of the beams in both connections. Connection A, which features bolts in a single row, exhibits a more linear moment-rotation relationship up to approximately 0.025 rad. In contrast, connection B, with a staggered bolt arrangement, demonstrates a more gradual and nonlinear moment-rotation relationship across the entire strain range. These suggest that the staggered bolt configuration provides a more gradual and progressive rotational stiffness than the single row bolt

TABLE 5: Mechanical properties of steel bolts.

Property	Expression	Value	Unit
Bolt grade	—	8.8	—
Yield strength	γ_{yb}	640	N/mm^2
Ultimate tensile strength	γ_{ub}	800	N/mm^2
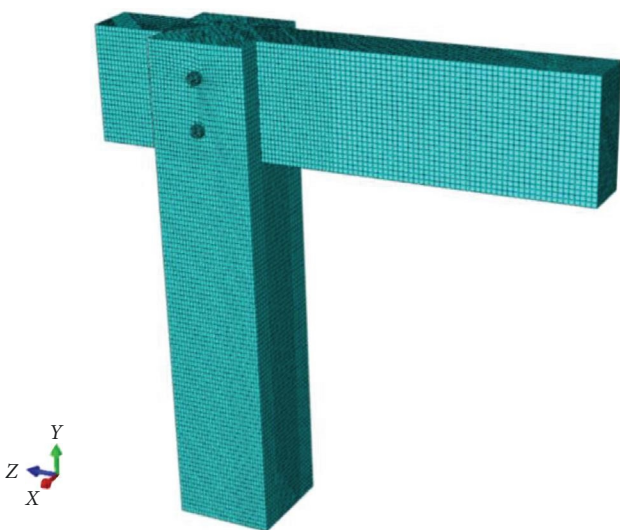
FIGURE 5: Connection A.

FIGURE 6: Connection B.

FIGURE 7: Moment-rotation curves for connections A and B of the roof beam to the column connection.

arrangement. Additionally, it also allows for some slip in the connection before the full moment resistance is mobilized.

At lower rotations (up to approximately 0.025 rad), the moment capacities of the two connections are similar. The difference in the moment-rotation curves of these two connections indicates that, increasing the moment, the single-row bolt arrangement (connection A) is able to perform a greater rotation capacity compared to the staggered bolt configuration (connection B). Figure 7 illustrates the moment-rotation curves for connections A and B.

A critical stress analysis of the timber members in connections A and B was performed, and the stress distribution associated with a displacement of 50 mm is illustrated in Figures 8 and 9, respectively. These figures indicate high-stress concentrations at the interface between the beam and the column. At the onset of failure, compressive stresses developed in the load-bearing region between the beams and columns, spreading to other parts of these members. This results in high compressive stresses perpendicular to the grain in the beams and peak compressive stresses parallel to the grain in the columns, ultimately leading to collapse. Therefore, failure of these connections is caused by excessive load-bearing and compressive stress perpendicular to the grain of the beam.

According to the European yield model (EYM) [20], the load-bearing capacities of connections A and B are governed partly by the failure mode j) in Figure 10.1 of [13], which represents the failure of the embedment in the central wooden element combined with the formation of a plastic hinge in the fastener. This yielding bolt failure was observed during the numerical analysis of both connections (Figure 10). The maximum Von Mises stress, $f_{max} = 647$ MPa, on the bolts exceeded the yield strength, $f_y = 640$ MPa, indicating irreversible plastic deformation of the bolts. Furthermore, the bolts in both connections did not fail simultaneously due to nonuniform stress distribution, highlighting the bolt group effect. Additionally, observations revealed that both bolts failed in connection A, while only a single bolt failed in connection B. From the stress distributions on the bolts in connection B, it was evident that only a single bolt is involved in the load transfer mechanism, explaining the lower load-bearing capacity of this connection compared to connection A.

The failure of connection A was compared to the failure of a double shear wooden connection obtained from experimental tests. The failure mode of connection A closely corresponds to that observed by Dietsch et al. [21] in their experimental studies. This failure is illustrated in Figure 11.
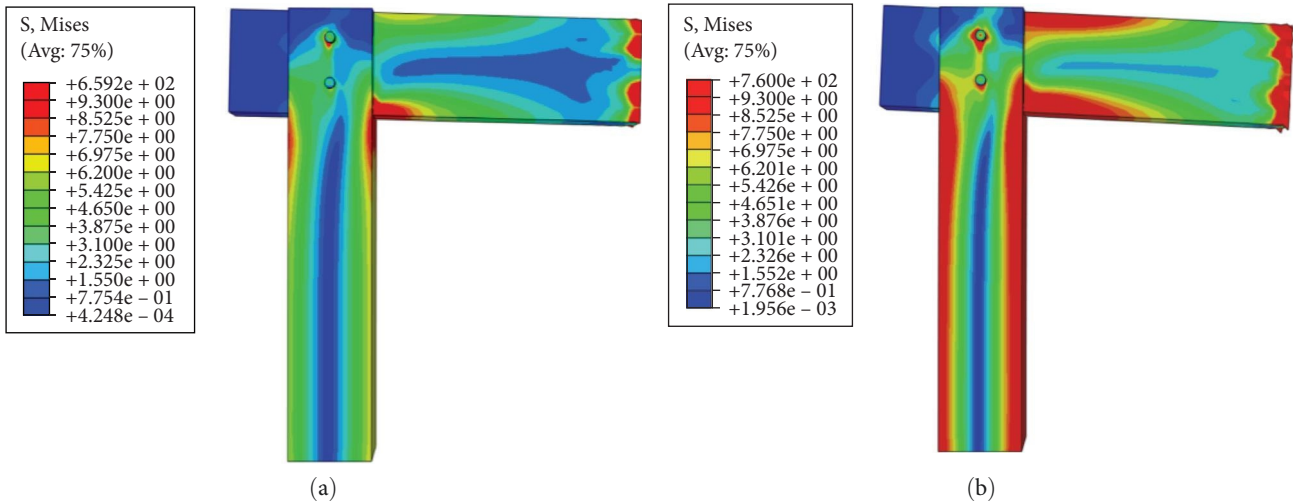
FIGURE 8: Stress distribution of connection A at the onset of failure (a) and at full failure (b).
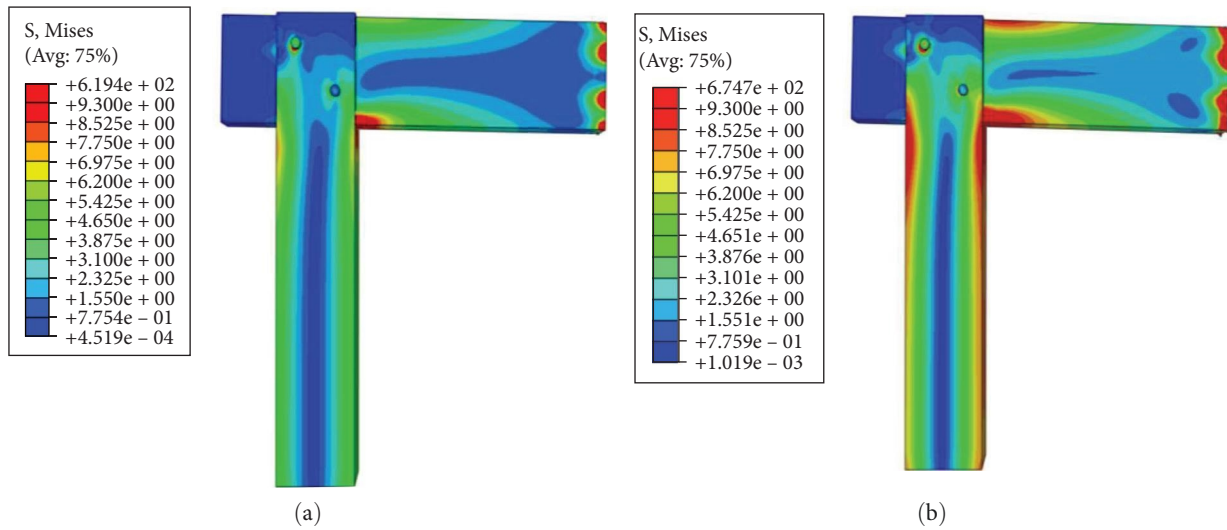
FIGURE 9: Stress distribution of connection B at the onset of failure (a) and at full failure (b).
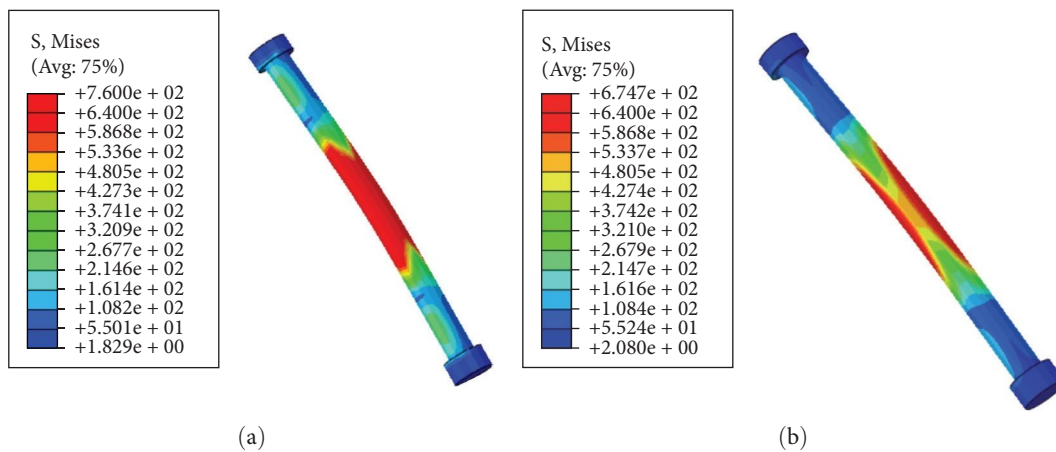
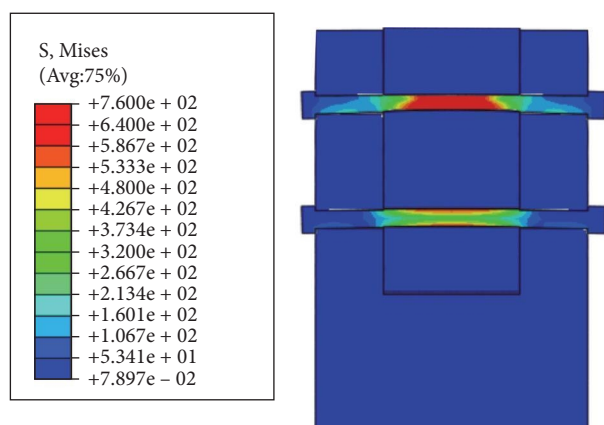FIGURE 10: Deformation of the bolts in connection A (a) and B (b).

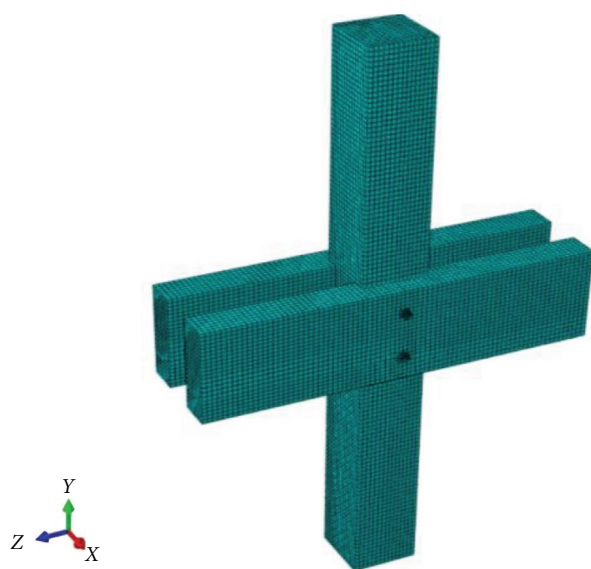FIGURE 11: Failure of connection A.

FIGURE 13: Load deformation curve of the double beam–column connection.

FIGURE 12: Numerical model of the double beam–column connection.

The staggered bolt arrangement is particularly advantageous in connections with smaller member sizes, where a single row of bolts may not be feasible. By arranging bolts in a staggered manner, the risk of creating high stress lines that could lead to cracking is minimized. This approach enhances load distribution across the connection and improves its structural integrity.

4.2. Double Beam-to-Column Connection. The numerical model developed for the double beam-column connection utilized C3D8R and C3D6 wedge finite elements for the wood and bolt mesh, respectively. With a maximum mesh size of 9 mm, a total of 103,908 finite elements were used for the numerical analysis of this connection. Figure 12 illustrates the numerical model of the double beam-column connection.

The load–deformation curve of the double beam-to-column connection (Figure 13) was obtained by applying a displacement of 50 mm at the two beam ends and a force of 35 kN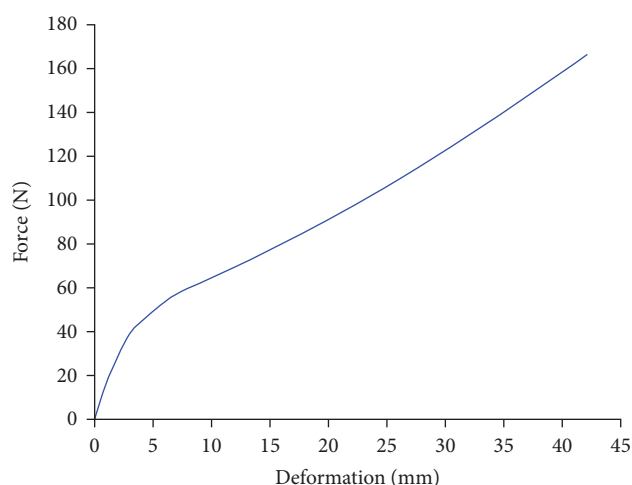 on the upper column. The curve exhibits a predominantly linear relationship between the load and deformation (elastic region) up to approximately 25% (40 kN) of the ultimate load. It also demonstrates the greatest stiffness in this elastic region. Beyond the 40 kN point, the curve starts to show a more nonlinear behavior suggesting the onset of plastic deformation or potential failure mechanisms within the connection. The curve then continues to demonstrate this nonlinear behavior, but with a gradually decreasing slope before reaching the maximum load capacity of around 160 kN. This could be attributed to progressive damage or yielding of the connection components. Additionally, the continuous increase in stiffness after the yield point may be due to the increased strength after the crushing of the wood fibers.

The relatively high stiffness during the initial phase of the loading can be attributed to the timber members being closely interlocked and bearing directly on each other. This implies that the connection can accommodate significant deformations before reaching its ultimate capacity. The nonlinear behavior beyond the yield point indicates that the connection can undergo some ductile deformation before potential failure.

The stress distribution on the wooden beams and columns is illustrated in Figures 14 and 15, respectively. At the onset of failure, peak compressive stresses developed at the interface (support point) between the double beams and columns. As the load increased towards failure, highly concentrated stresses spread throughout the timber members, creating peaks in compressive stresses perpendicular to the beam grain, ultimately leading to connection failure. Additionally, distortion of the mesh around the bolts was observed, indicating local crushing of the wood around the bolts under the applied displacement. It can also be noted that the upper and lower columns did not fail, suggesting that the failure of the double beam-column connection is primarily due to excessive compressive stresses perpendicular to the grain developed in the beam.

The stress distribution plots on the bolts indicate that the bolts did not reach their yield point at the connection failure point. The bolts are not directly subjected to shear, but function to position the beams and columns. However, stress values suggest the possible formation of a plastic hinge in the fastener

(a)   (b)
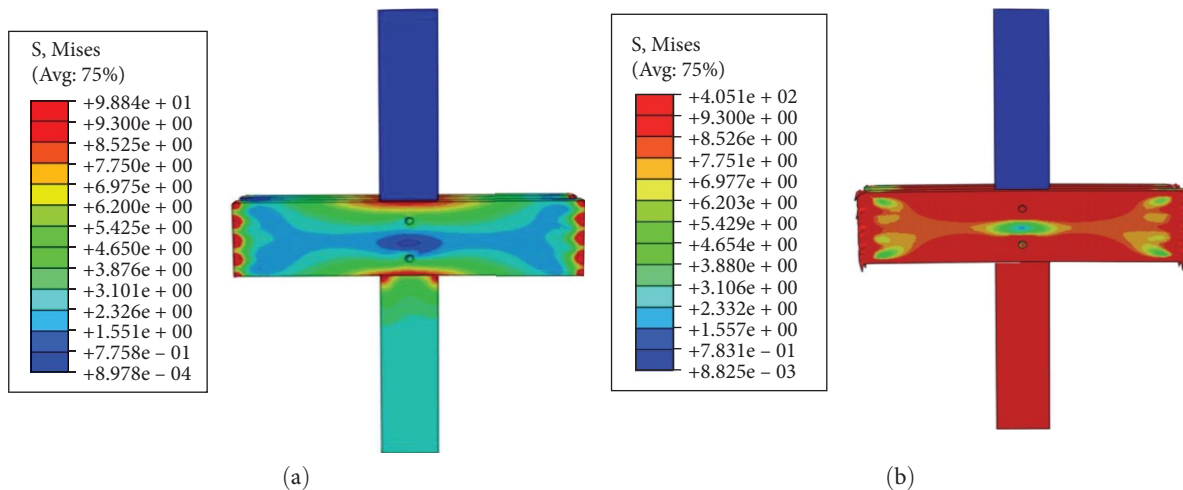
FIGURE 14: Stresses distribution on wooden beams: at onset of failure, (a) and at full failure (b).
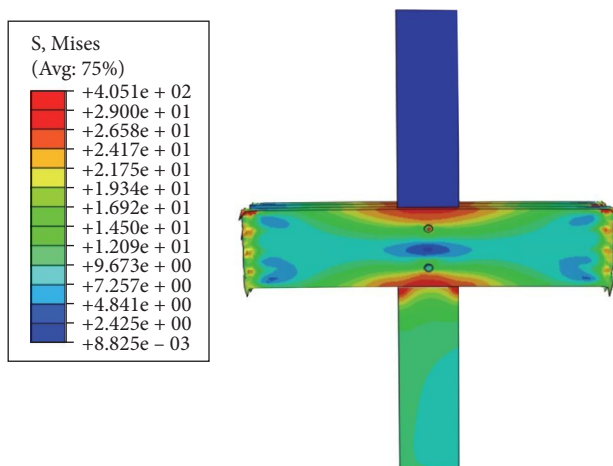

FIGURE 15: Stresses distribution on wooden columns upon failure of the double beam–column connection.

on the central column member. This bolt failure mode agrees well with the design assumption and the failure mode (j) in Figure 10.1 of [13]. The bolt deformation in the double beam-column connection is illustrated in Figure 16.

A parametric study was conducted to investigate the influence of a gap between the upper wooden column and the double beams on the overall behavior of the connection. The upper column could potentially induce greater compressive stresses perpendicular to the grain of the double beams. To explore this, a gap of 10 mm was introduced between the top column and the double beams to study its effect. The results of the numerical analysis revealed that introducing a gap did not significantly affect the load transmission or overall bearing capacity of the connection. A gap of at least 10 mm in the double beam-column connection can be beneficial in fire situations, as it may reduce the conductive spread of fire between the structural elements of the connection. Figure 17 illustrates the stress distribution on the double beam connection with a gap between the top column and the double beams.

The negligible impact on the structural performance of the connection, when a 10 mm gap is introduced between the double beams and the upper column can be advantageous in fire scenarios. This gap reduces the conductive heat transfer between the wooden elements to a certain extent. Additionally, it can decrease the time required for water to flow through the connection, thereby reducing the risk of swelling and shrinking of the connection components. Finally, the similar structural performance of the double beam-column connection compared to a single beam connection allows for simpler connection systems (i.e., bearing on the columns), beams of reduced depth, and provides spaces for the arrangement of MEP systems between the double beams.

4.3. Connection at the Base of the Column. Two numerical models, namely connection C and connection D, were developed for the connection at the base of the wooden column to study the influence of a gap between the top of the wooden column and slotted in base plate. Connection C featured a 10 mm gap between the top of the wooden column and the slotted in base plate, while connection D had the wooden column overlapping the base plate at the top contact surface. The wood elements and base plate connector were meshed with C3D8R finite elements, and C3D6 wedge elements were used for the bolts. With a maximum mesh size of 9.5 mm, the number of finite elements in both connections was 82,272 and 80,614, respectively. The numerical models of connections C and D are shown in Figure 18. Additional models of these connections, highlighting the gap are illustrated in Figure 19.

The load-deformation curves of connections C and D were obtained by applying a displacement of 50 mm at the top of the wooden columns to simulate the behavior of these connections under axial loading. The load–deformation curve of connection C exhibits relatively linear behavior up to approximately between 3 and 5 mm deformation. Beyond this point, the curve begins to deviate from linearity, indicating the onset of plastic deformation within the connection. The maximum load capacity for the connection is approximately between 150 and 160 kN.
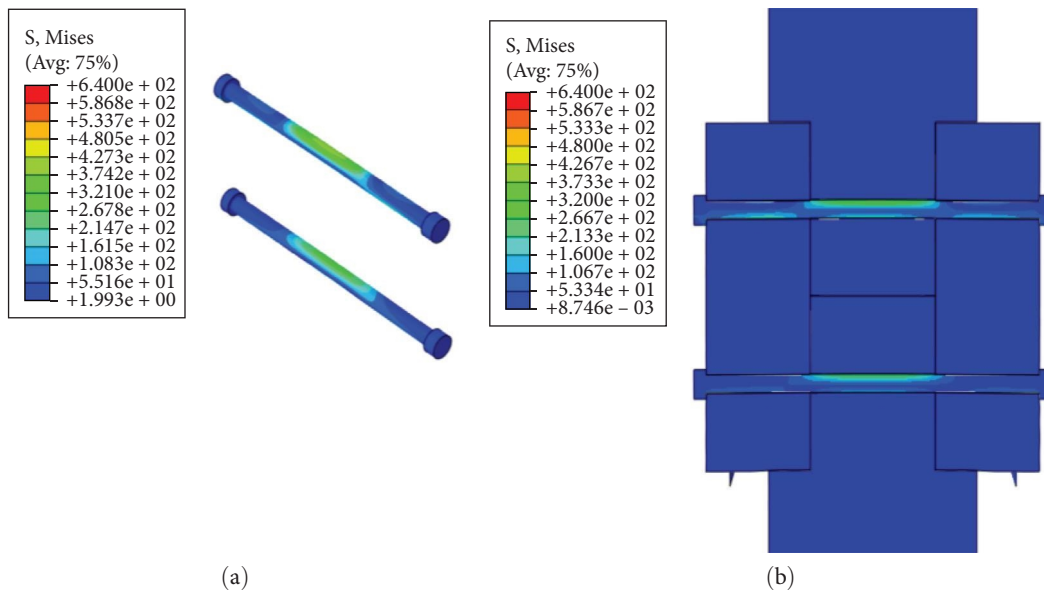
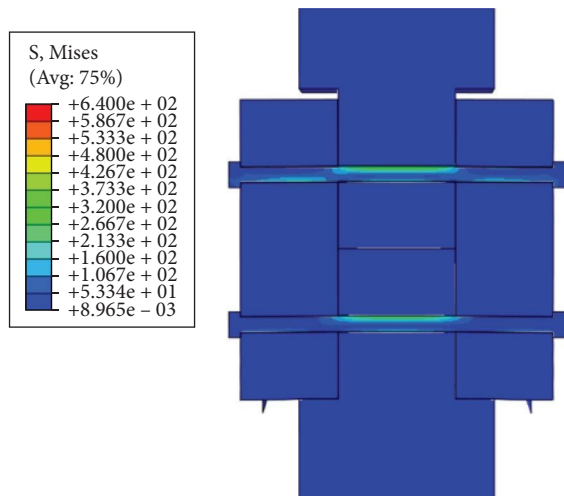FIGURE 16: Deformation of the bolts (a) in the double beam–column connection (b).

FIGURE 17: Stress distribution on the bolts of the connection between double beam and column with gap.

Connection D, on the other hand, has a steeper but nearly equal initial stiffness compared to connection C up to the yield point of around 120 kN. Beyond this point, the curve exhibits a more gradual transition into the nonlinear region, followed by a plateau formation, after which a sharp drop in force occurs. The continuous increase in deformation of connection D, after the yield point, suggests that ductile behavior is more pronounced and it can withstand larger deformations before reaching its maximum capacity. In contrast, connection C shows a sudden collapse.

The load deformation curves of connections C and D are presented in Figure 20.

A stress analysis of the wooden column in connections C and D was performed to evaluate the stress distribution in the wooden columns. In connection C, the initial failure of the wooden column begins at the base of the column with a load of 62.30 kN. Compressive stresses parallel to the grain then spread throughout the column, leading to the failure of the entire column. This initial failure is caused by the deformation of the wood fibers at the base of the column, which is in contact with the base plate. In connection D, plastic deformations in the wooden column first appear at the interface between the slotted in base plate under a load of 44.37 kN, and subsequently, spread throughout the column. Gapless connections create concentrated stresses at the interface between the column and the slotted in base plate, resulting in wood failure at a significantly lower load compared to connections with gaps of 10 mm. The stress distribution on the wooden columns at the onset and full failure in connections C (with a gap of 10 mm) and D is illustrated in Figures 21 and 22, respectively.

Even though in Figure 21 stresses can be observed at the location of the gap, they are quite small and approximately equal to 0.4 MPa. This value is seven times less than the stresses in the observed in the connection without a gap. Clearer detail of the connection C can be seen in Figure 19. Higher stresses observed at the onset of failure in connection C and D means that connection C has a higher failure load than connection D.

The stress distribution on the slotted in base plate connector in connection C indicates that the steel has not failed except in areas of high stress concentration, such as around the bolt holes. The stress values in most parts of the plate did not exceed the maximum stress of 127 MPa, implying reversible deformation of the steel base plate in connection C. In connection D, however, the base plate is extensively fractured in most areas, with stress values reaching up to 290 MPa, indicating an irreversible deformation of the steel plate. The failure of the base plate in connection D is attributed to its active participation in the transmission of the axial load. It is important to note that the columns of connection C and D remain under very low stress, very low stresses even when the connections fail. Therefore, the failure is caused by excessive yield stresses parallel to the grain of the wooden column or by a combination of these
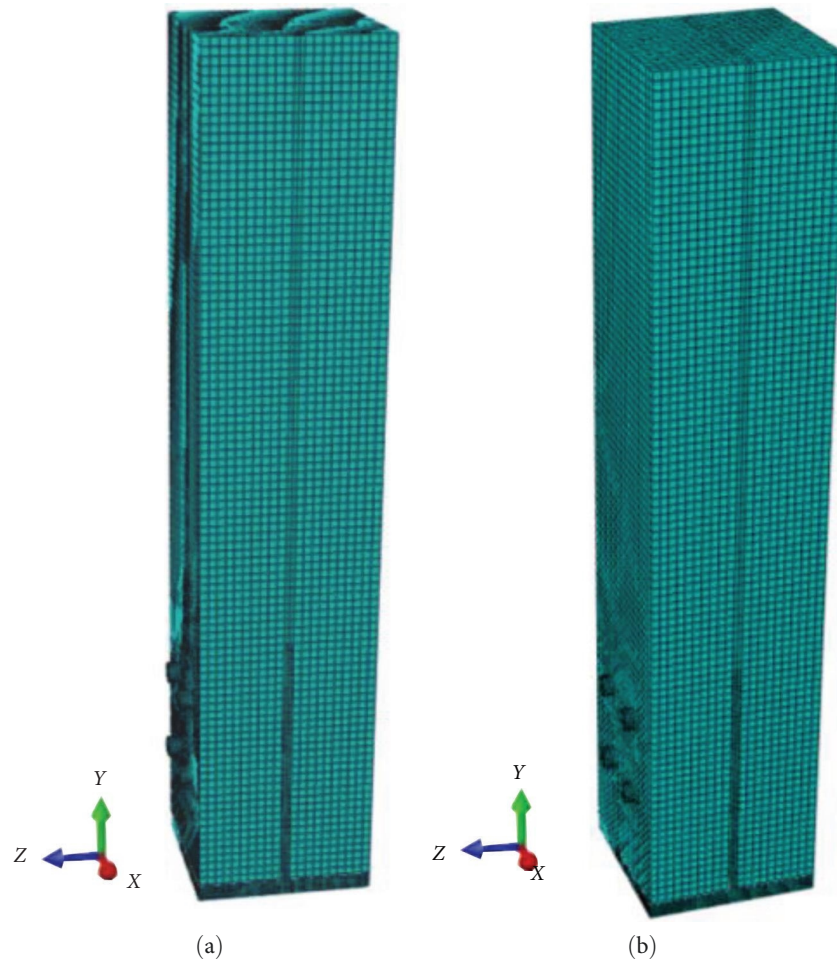
(a)   (b)

FIGURE 18: Numerical models of connection C (a) and D (b).
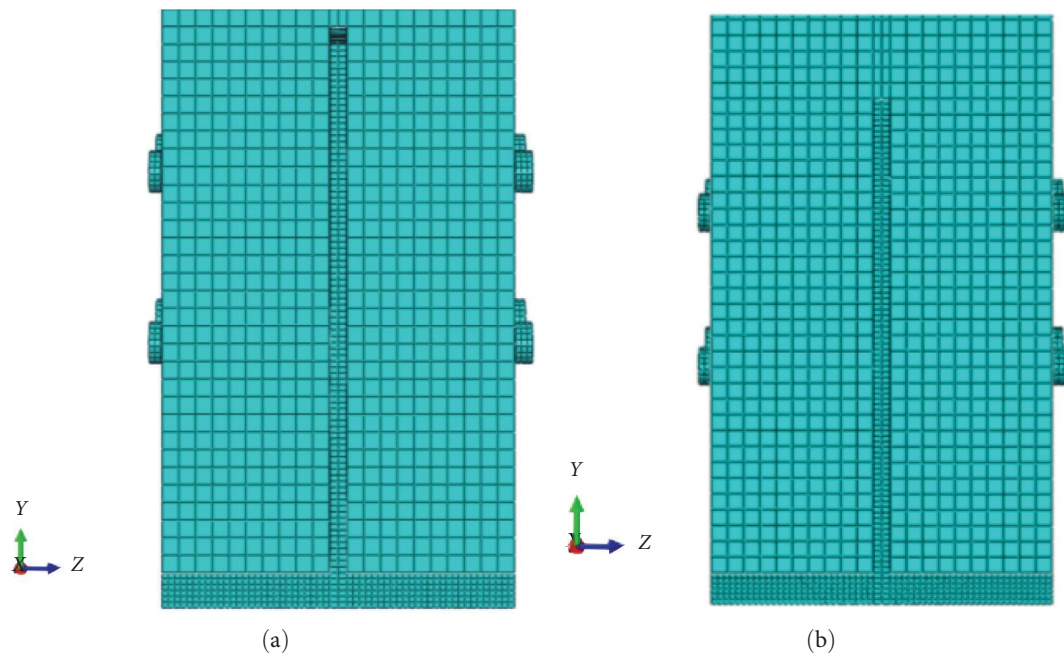

(a)   (b)

FIGURE 19: Details of the connection of C with a gap (a) and of D without a gap (b).
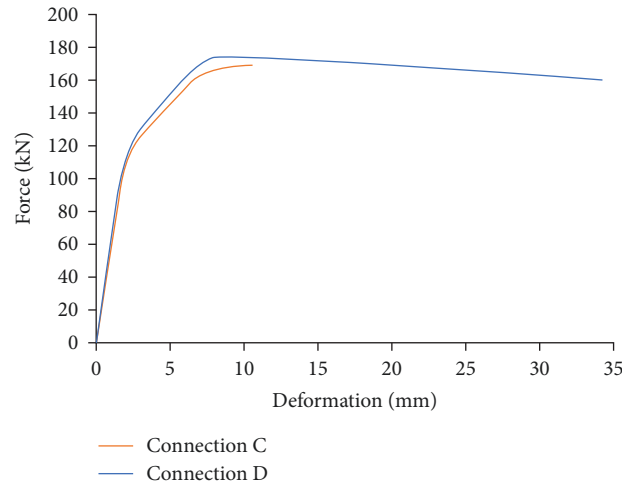
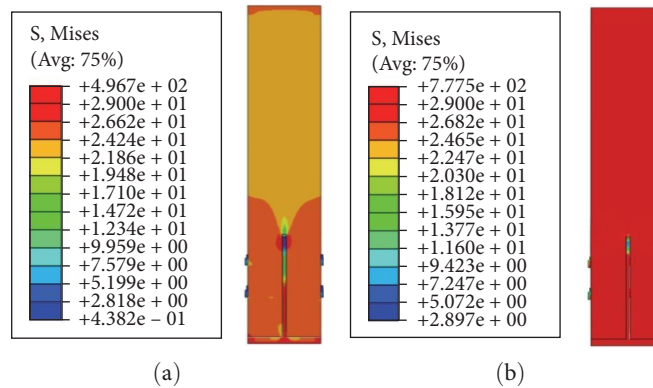FIGURE 20: Load deformation curve of wooden base connection.

FIGURE 21: Stress distribution at the beginning of the failure of wooden column in connection C (a) and at full failure (b).
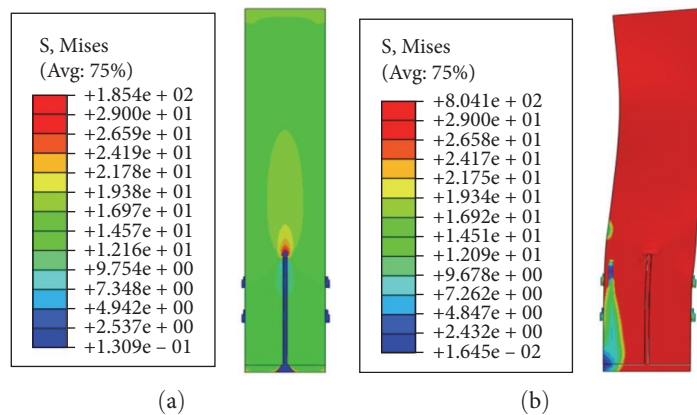

FIGURE 22: Stress distribution at the beginning of the failure of wooden column in connection D (a) and at full failure (b).

stresses and the yield stress of the base plate. Furthermore, the load transfer mechanism consistent with the design assumptions is demonstrated by connection C. This further reinforces the advantage of incorporating a gap of 10 mm between the top of the slotted in base plate and the wooden column. The stress distribution at failure on the slotted in base plate connectors in connections C and D is illustrated in Figure 23.

The load-bearing capacities of these connections are governed partly by the failure mode g in Figure 10.1 of [13], which represents the formation of a plastic hinge in the central steel
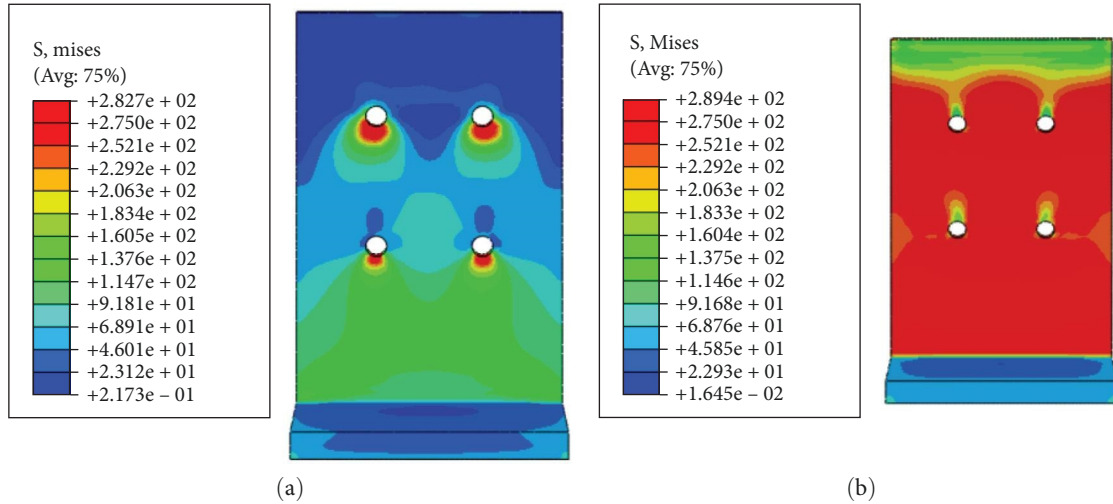
FIGURE 23: Stress distribution at failure on the steel slotted in base plate in connection C (a) and D (b).
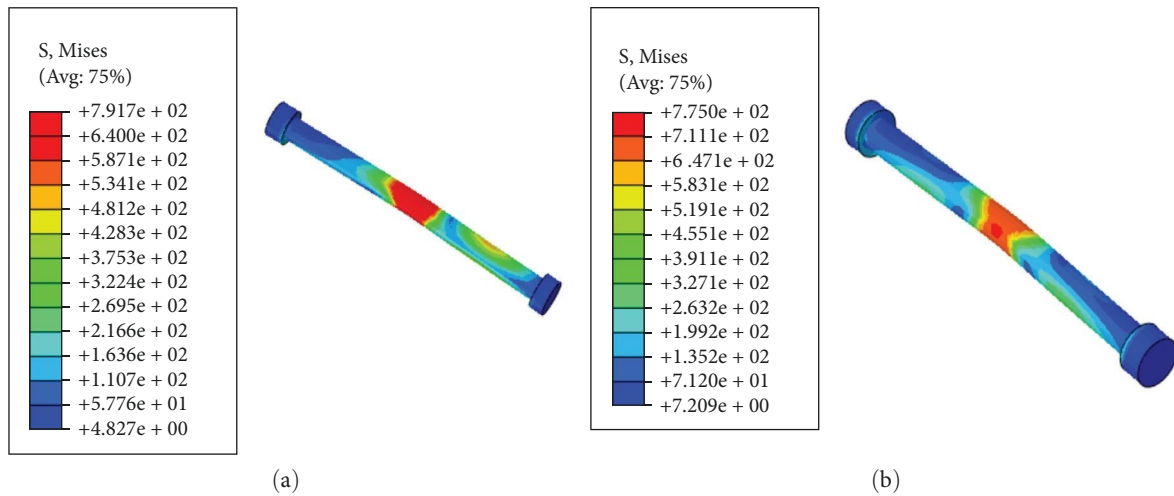

FIGURE 24: Deformation of bolts in connections C (a) and D (b).

member. This bolt failure was observed to a limited extent during the numerical analysis of connections C and D (Figure 24). The maximum Von Mises stress, $f_{max} = 645$ MPa on the bolt exceeded the yield strength, $f_y = 640$ MPa, indicating irreversible plastic deformation of the bolt.

The deformation of the bolts and base plate connector in connections C and D is illustrated in Figure 25. The bending behavior of the wooden column in connection D can also be observed, which is attributed to the deformation of the base plate connector under high axial compressive loads. In contrast, the column in connection C remains straight and vertical.

Based on these results, introducing a 10 mm gap in the wooden base connections may offer practical advantages. First, it reduces narrow margins of error and improves manufacturing tolerances during the assembly of connections. Second, it can enhance the fire resistance time of these connections by minimizing the contact points between the slotted in base plate and wood.

4.4. Areas of Possible Convergence Issues and Solutions. In typical applications involving bolted timber connections, a maximum tolerance of 1 mm is often allowed, to overcome the tight margins required for aligning holes and fitting bolts. One primary reason these tolerance gaps are used in wood connections is to prevent splitting of the wood connection members and for easy assembling. Removing the tolerance gap does not affect the accuracy of the numerical results.

However, implementing this tolerance in the numerical models can lead to convergence problems as contact, a necessary step in the simulation process, must be established between touching components. To overcome this problem, it was decided to make the dimensions of holes and bolts equal.

5. Comparison of Numerical Results With Experimental Ones

The bolt failure modes of the roof beam-to-column, double beam-to-column, and timber base connections (Figures 10,
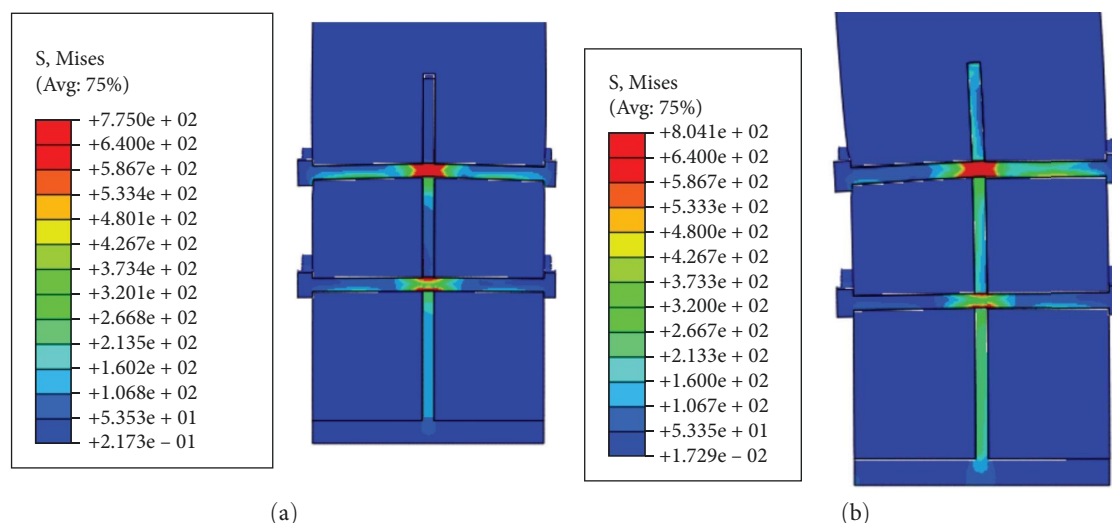
FIGURE 25: Deformation of bolts and slotted in base plate in connections C (a) and D (b).

16, and 24) obtained from the finite element models are compared to experimental bolt failure modes in Figure 4 of [22]. These experiments were conducted on double-shear timber connections with slotted in steel plates subjected to shear stresses and closely resemble the geometry and loading of the timber base connection. This comparison was performed to validate the double-shear beam-to-column connections, as they later were designed according to Eurocode 5 for both bearing—timber-to-timber contact—and shear bolts, making this comparison logical. To further support the second comparison, the failure modes of the beam-to-column connections and timber base connection were also analyzed against the proposed failure modes, that is, (j) in Figure 10.1 of [13] and (g) in Figure 10.2 of [13] used in the design of these connections.

The predictions from the finite element models demonstrate reasonably good agreement with the experimental data in terms of capturing the bolt failure modes. The deformation and formation of plastic hinges in the central parts of the bolts closely correspond with both experimental and theoretical predictions. However, the model did not account for failures in the wood around the dowel holes, such as crushing. This limitation arises because the connections were studied up to failure without considering postfailure and brittle failure modes, such as cracking and crushing. Instead, a pressure overclosure relationship was applied to account for the softening behavior of wood round the bolt holes. Figure 4 of [22] illustrates the failure of a double shear timber-to-timber connection with slotted in plates subjected to shear forces.

6. Conclusions

This work aimed to analyze the mechanical behavior of hybrid steel–wood hybrid connections in wooden residential buildings using the finite element method. Prior to developing detailed 3D models of the connections in the case study building, a rigorous structural analysis was performed on the building to ensure that the structural elements and connections met strength and durability conditions. At this stage, critical connections in buildings were designed using simplified expressions obtained from Eurocode 5. The configurations of these connections were adapted from existing literature to meet specific requirements of the building.

Subsequently, nonlinear finite element models were developed for three main connections using the Abaqus/CAE Implicit solver. These connections included wood roof beam-to-column connections, double wood-beam-to-column connections, and wood-column-to-concrete column connections. These models incorporated combined anisotropic yielding and ductile fracture of wood, particularly near bolt holes, using the Hill criterion coupled with the Dorn pressure overlocking relationship. The yield strength of steel components (bolts and slotted in base plates) was also considered using the Von Mises failure theory.

The numerical models were subjected to monotonic displacement of 50 mm at appropriate connection points to evaluate their behavior. The numerical results for some connections were validated against the experimental data, while the validation of other models was based on the bolt failure mode proposed by Eurocode 5. From the numerical results, the models were able to adequately predict bolt failure and yield strength to a reliable extent of steel and wooden elements of the connections. Several conclusions could be drawn from the numerical modeling, as listed below:

1. The failure of the load-bearing wooden beam-column connections is mainly due to compressive stress peaks perpendicular to the grain of the beams.

2. Single-row bolt configurations in timber load-bearing connections improve ductility and provide greater moment-resisting capacity than staggered bolt configurations.

3. Bolts in wooden connections subjected to monotonic loading fail at different stages of the applied load.

4. The fasteners in the double wooden beam-column connections play a limited role in the load transfer mechanism.

5. Introducing a large gap can reduce contact between the two connection components and possibly result in rotation of the timber column around the base plate; for example, connections at the base of wooden columns with slotted in base plates with a gap of at 10 mm between the top of the slotted in base plate and column demonstrate superior ductility and performance compared to connections without gaps.

These findings have the potential to inform reliable and efficient design for wooden connections, if implemented appropriately.

Other configurations are either derivatives or mirrors of these two basic setups and might not affect the results much differently.

To solidify their applications, future research work can verify these findings by using other useful hardwood species. Further, numerical simulations can also be performed on different bolt arrangements and component configurations in these connections.

Data Availability Statement

The data will be available upon request from the authors.

Conflicts of Interest

The authors declare no conflicts of interest.

Funding

References

[1] H. Eslami, L. B. Jayasinghe, and D. Waldmann, "Nonlinear Three-Dimensional Anisotropic Material Model for Failure Analysis of Timber," *Engineering Failure Analysis* 130 (2021): 105764.

[2] P. Niemz, A. Teischinger, and D. Sandberg, *Springer Handbook of Wood Science and Technology* (Springer, 2023): 2064.

[3] B. H. Xu, A. Bouchaïr, M. Taazount, and E. J. Vega, "Numerical and Experimental Analyses of Multiple-Dowel Steel-to-Timber Joints in Tension Perpendicular to Grain," *Engineering Structures* 31, no. 10 (2009): 2357–2367.

[4] B. H. Xu, M. Taazount, A. Bouchaïr, and P. Racher, "Numerical 3D Finite Element Modelling and Experimental Tests for Dowel-Type Timber Joints," *Construction and Building Materials* 23, no. 9 (2009): 3043–3052.

[5] J. M. Cabrero, B. Iraola, and M. Yurrita, "Failure of Timber Constructions," in *Handbook of Material Failure Analysis*, eds. A. S. H. Makhlouf and M. Aliofkhazraei, (Oxford, UK, Butterworth-Heinemann, 2018): 123–152.

[6] E. F. Hansson, "Analysis of Structural Failures in Timber Structures: Typical Causes for Failure and Failure Modes," *Engineering Structures* 33, no. 11 (2011): 2978–2982.

[7] Task Commitee on Fastners of the Commitee on Wood of the Structural Division of the American Society of Civil Engineers (ASCE), *Mechanical Connections in Wood Structures: Manuals and Reports on Engineering Practice* (American Society of Civil Engineers, New York, 84, 1996).

[8] J. Porteous and A. Kermani, *Structural Timber Design to Eurocode 5* (Blackwell Publishing, 2008).

[9] CEN, EN 1995-1-1:2004 Eurocode 5, *Design of Timber Structures. Part 1-1: General Rules and Rules for Buildings* (European Committee for Standardisation).

[10] P. Racher, J. P. Biger, F. Rouger, G. Sagot, and G. Vidon, *Introduction à l'Eurocode 5, matériaux et bases de calcul: Structures en bois aux états limites*, (1996).

[11] AWC's Wood Design Standards Committee, *National Design Specification (NDS) for Wood Construction*, (2024).

[12] K. W. Johansen, *Theory of Timber Connections* (IABSE Publications, 1949).

[13] Swedish Wood, "Design of Timber Structures," in *Rules and Formulas According to Eurocode 5*, 2, Third Revised edition, (2022).

[14] Swedish Wood, "Design of Timber Structures," in *Rules and Formulas According to Eurocode 5*, 1, Third Revised edition, (2022).

[15] A. Hassanieh, H. R. Valipour, M. A. Bradford, and C. Sandhaas, "Modelling of Steel-Timber Composite Connections: Validation of Finite Element Model and Parametric Study," *Engineering Structures* 138 (2017): 35–49.

[16] A. O. Cifuentes and A. Kalbag, "A Performance Study of Tetrahedral and Hexahedral Elements in 3D Finite Element Structural Analysis," *Finite Elements in Analysis and Design* 12, no. 3-4 (1992): 313–318.

[17] K. Laplanche, *Etude du Comportement au feu des Assemblages de Structures Bois : Approche Expérimentale et Modélisation* (Université Blaise Pascal, Clermont, p. 146, 2006).

[18] R. Hill, "A Theory of the Yielding and Plastic Flow of Anisotropic Metals," *Proceedings of the Royal Society of London, Series A, Mathematical and Physical Sciences* 193, no. 1033 (1948): 281–297.

[19] CEN, EN 338, 2009 Structural Timber, "Strength Classes, European Committee for Standardisation," (Strength Classes

[20] L. A. Soltis, "European Yield Model For Wood Connections, Structures Congress '91 Compact Papers," in *9th Structures Congress Proceedings*, (Indianapolis, IN. New York: American Society of Civil Engineers, 1991), 60–63.

[21] P. Dietsch, S. Schmid, M. Merk, and S. Winter, "Cinematic Visualization of Failure Mechanisms in Timber Structures," in *WCTE World Conference on Timber Engineering*, (Riva del Garda, Italy, 2010).

[22] C. Sandhass and J.-W. G. van de Kuilen, "Strength and Stiffness of Joints With Very High Strength Steel Dowels," *Engineering Structures* 131 (2017): 394–404.